Applied Catalysis B: Environmental 113–114 (2012) 43–51

Contents lists available at SciVerse ScienceDirect

Applied Catalysis B: Environmental

journal homepage: www.elsevier.com/locate/apcatb

Study of N-bridged diiron phthalocyanine relevant to methane oxidation: Insight into oxidation and spin states from high resolution 1s core hole X-ray spectroscopy

Evgeny V. Kudrik[a,b], Olga Safonova[c], Pieter Glatzel[c], Janine C. Swarbrick[c], Leonardo X. Alvarez[a], Alexander B. Sorokin[a,*], Pavel Afanasiev[a,*,1]

[a] Institut de Recherches sur la Catalyse et l'Environnement de Lyon, IRCELYON, UMR 5256, CNRS – Université Lyon 1, 2, av. A. Einstein, 69626 Villeurbanne, France
[b] Ivanovo State University of Chemistry and Technology, 7, av. F. Engels, 153000 Ivanovo, Russia
[c] European Synchrotron Radiation Facility (ESRF), 38043 Grenoble 9, France

ARTICLE INFO

Article history:
Available online 25 November 2011

Keywords:
Iron phthalocyanine
μ-Nitrido dimer
Methane oxidation
X-ray spectroscopy
XES
RIXS

ABSTRACT

μ-Nitrido diiron phthalocyanine $[PcFe^{+3.5}NFe^{+3.5}Pc]^0$ is a highly efficient catalyst, able to oxidize methane under near-ambient conditions. In this work, high resolution X-ray emission spectroscopy (XES) and resonant inelastic X-ray scattering (RIXS) were applied to study iron species in the series of μ-nitrido diiron phthalocyanines including initial $[PcFe^{+3.5}NFe^{+3.5}Pc]^0$ and oxidized complexes $[PcFe^{IV}NFe^{IV}Pc]^+PF_6$ and $[PcFe^{IV}NFe^{IV}(Pc^{\bullet+})]^{2+}Br_2$ as model compounds for the intermediates in the catalytic cycle. These systems contain $3d^4$ configuration of iron in high oxidation state Fe(IV). XES spectra of Kβ line are sensible to the local iron spin density and show unexpected difference in the spin state between the initial $[PcFe^{+3.5}NFe^{+3.5}Pc]^0$ (LS), one-electron oxidized $[PcFe^{IV}NFe^{IV}Pc]^+PF_6$ (HS) and two electron oxidized cation radical species $[PcFe^{IV}NFe^{IV}(Pc^{\bullet+})]^{2+}Br_2$ (LS). Fe K-edge XANES spectra were recorded at the fluorescence energy of the main $K\beta_{1,3}$ line or Kβ′ line in the Kβ emission spectrum. The conclusions of RIXS study corroborated XES data. Our study suggests that the main catalytic pathway of oxidation includes two-electron transformation from the LS initial complex to the LS two–electron oxidized $[PcFe^{IV}NFe^{IV}(Pc^{\bullet+})(O)]^0$ to generate powerful oxidant able to oxidize methane via two-electron process.
© 2011 Elsevier B.V. All rights reserved.

1. Introduction

Along with traditional high temperature approaches to utilization of methane [1–3], low temperature conversion of methane is a long standing challenge both from fundamental and practical point of view. For a long time this approach has been associated with activation of CH_4 at transition metal centers like Pt, Pd, Ir, etc. [4–6]. So far, the most efficient system is based on platinum which operates at 220 °C in oleum, converting CH_4 to CH_3OSO_3H [5,6]. Relatively high temperatures (100–220 °C) and strong concentrated acids (oleum, CF_3COOH) are generally needed for activation of methane by this approach.

We have recently proposed to use binuclear iron complexes with macrocyclic porphyrin-like ligands as catalysts for oxidation of strong C–H bonds [7–14]. This concept was inspired by biochemical precedents of difficult oxidation reactions performed by soluble methane monooxygenase (MMO) [15] and cytochrome P-450 enzymes [16] containing diiron non-heme and iron porphyrin sites, respectively. These enzymes generate powerful oxidizing species capable of oxidizing even methane (MMO) under very mild conditions (water medium, ambient temperature).

Combining structural features of two enzyme families we have put two iron atoms connected via μ-nitrido bridge in macrocyclic ligand environment. These N-bridged diiron porphyrin and phthalocyanine complexes have been described in literature [17,18] but no catalytic applications of them have been reported prior to our work. We have recently demonstrated that N-bridged diiron tetra(tert-butyl)phthalocyanine complex containing Fe^{III}–N=Fe^{IV} structural unit activated H_2O_2 leading to a very strong oxidizing species which oxidized methane in water at 25–60 °C [7,8]. The same system catalyzes oxidation of propane and ethylene [12] as well as benzene [9] and alkylaromatic compounds [11]. Therefore such binuclear macrocyclic complexes represent a novel and promising scaffold in the oxidation catalysis. The importance of the low temperature oxidation of light hydrocarbons, including methane, determines the interest to the mechanistic aspects and the structure of the active species. Available spectroscopic and reactivity data indicate the retention of Fe–N–Fe binuclear

* Corresponding authors. Tel.: +33 472 445 337; fax: +33 472 534 499.
E-mail addresses: alexander.sorokin@ircelyon.univ-lyon1.fr (A.B. Sorokin), pavel.afanasiev@ircelyon.univ-lyon1.fr (P. Afanasiev).
[1] Tel.: +33 472 445 466; fax: +33 472 534 499.

0926-3373/$ – see front matter © 2011 Elsevier B.V. All rights reserved.
doi:10.1016/j.apcatb.2011.11.028

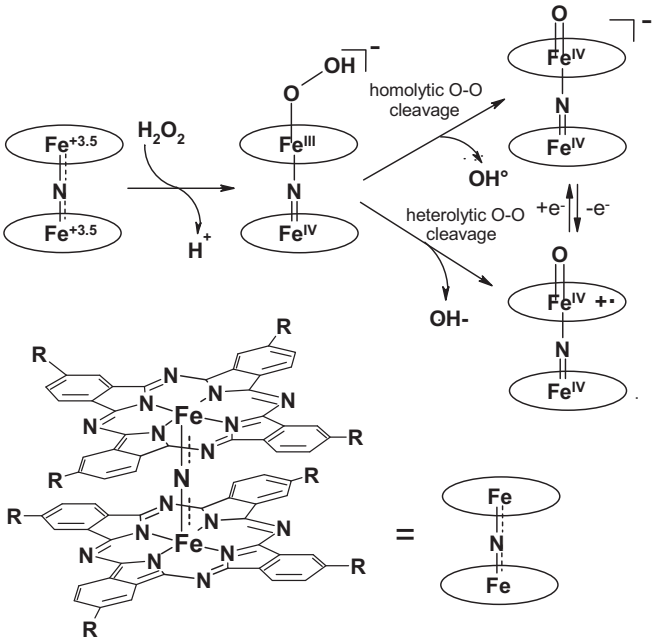

Fig. 1. Possible high-valent diiron oxo complexes formed in the presence of hydrogen peroxide. R = H (this work), R = t-Bu (Refs. [7,8]).

structure during catalytic cycle and possible involvement of high-valent diiron oxo complexes as oxidizing species (Fig. 1).

Two iron sites of the starting diiron complex are equivalent according to the presence of only one doublet in Mössbauer spectrum ($\delta = 0.06\,mm\,s^{-1}$, $\Delta E_Q = 1.76\,mm\,s^{-1}$ at 77 K) and the structure can be described as Fe(+3.5)NFe(+3.5) [18]. At the first step the $PcFe^{+3.5}NFe^{+3.5}Pc$ forms hydroperoxo complex which can undergo either homolytic or heterolytic cleavage of O–O bond resulting in $[PcFe^{IV}NFe^{IV}(O)Pc]^-$ (in combination with $OH^\bullet$) or $[PcFe^{IV}NFe^{IV}(O)(Pc^{\bullet+})]$ oxo complexes. Both pathways lead to strong oxidizing species. There is a significant difference of this diiron system from those previously described in the literature. Enzymatic and model iron-based systems activate dioxygen or active oxygen donors like H_2O_2 with the help of iron species in the low oxidation state of +2 or +3 to generate Fe(+4) species which can contain ligand cation-radical providing an additional redox equivalent. In contrast, Fe oxidation state in the initial N-bridged diiron complex is already +3.5. From viewpoint of generally accepted mechanistic paradigm of reactivity this complex should not be active in activation of H_2O_2 to generate active oxo species via $2e^-$ pathway.

Thus, the mechanistic features of the formation of a powerful active species capable of oxidizing methane are far from being fully understood. During generation of the diiron active species the iron atoms of the complex change the oxidation and spin states to form transient elusive species. However, a direct investigation of these species is a very challenging task because of high reactivity and, hence, extreme instability of these species. Several stable high valent diiron complexes in the same oxidation states without oxo ligand have been obtained on the unsubstituted phthalocyanine platform [17–19]. These stable diiron complexes can be considered as isoelectronic analogues of unstable oxo diiron complexes involved in oxidation of the strong C–H bonds. In order to get insight into oxidation and spin states of iron atoms in these species we have prepared $[PcFe^{+3.5}NFe^{+3.5}Pc]^0$ (**1**), $[PcFe^{IV}NFe^{IV}Pc]^+PF_6$ (**2**) and $[PcFe^{IV}NFe^{IV}(Pc^{\bullet+})]^{2+}Br_2$ (**3**). The complexes **2** and **3** can be considered as model complexes for $[PcFe^{IV}NFe^{IV}(O)Pc]^-$ and $[PcFe^{IV}NFe^{IV}(O)(Pc^{\bullet+})]$ intermediates, respectively, which can be formed during catalytic cycle. The state of iron atoms in **1**–**3** has been probed by high resolution X-ray emission spectroscopy (XES) and resonance inelastic X-ray scattering (RIXS).

During the last years, core hole spectroscopies using synchrotron radiation, including EXAFS/XANES, XES and RIXS showed their great utility to address the problems of the state of iron in various fields, from biochemistry of iron-containing enzymes [20] to the studies of iron in the mantle minerals under extreme conditions [21]. Much effort was directed to the understanding of iron state in the heterogeneous catalysts [22,23] and model iron complexes, both heme [24,25] and non-heme [26–28] structures. An introduction to these techniques and their applications to resolving chemical problems is given in the reviews [29,30]. In the present work we provide an account of XES and RIXS study of the non-substituted phthalocyanine N-bridged diiron model complexes **1**–**3** mimicking the reaction intermediates during catalytic cycle of methane oxidation. The possible relationship between electronic state of iron determined by XES and RIXS and catalytic properties of N-bridged diiron complexes is discussed.

2. Materials and methods

2.1. Preparation of complexes

Iron(III) phthalocyanine chloride (FePcCl, 95% purity) obtained from Sigma–Aldrich was purified by the treatment with concentrated HCl to remove impurities and to transform the traces of μ-oxo dimer to FePcCl. Then the product was washed with water until neutral pH and dried. μ-Nitrido-bis(phthalocyaninatoiron) ($[PcFe^{+3.5}NFe^{+3.5}Pc]^0$, (**1**) [17], one-electron oxidized $[PcFe^{IV}NFe^{IV}Pc]^+PF_6$ (**2**) [19] and two electron oxidized $[PcFe^{IV}NFe^{IV}(Pc^{\bullet+})]^{2+}Br_2$ (**3**) [31] were prepared according to published protocols. Their spectroscopic properties were the same as those published in literature.

2.2. Catalytic experiments

For the catalytic study, complex **1** was supported onto silica (Degussa, Aerosil 300) preliminary dried in vacuum at 200 °C during 8 h. Complex **1** (62 mg) was stirred with 600 mL CH_2Cl_2 during 6 h. After addition of silica (5 g) the reaction mixture was stirred at 25 °C until all complex was absorbed onto silica and the solution became colorless. The supported catalyst was isolated by filtration, washed with CH_2Cl_2 (3×50 mL) and dried in vacuum at 80 °C for 6 h. The catalyst loading was 10.8 μmol/g. Oxidation of methane was performed as previously described [8].

2.3. X-ray emission and scattering experiments

The experiments were performed on the high brilliance X-ray emission beamline ID26 at the ESRF. The electron energy was 6.0 GeV with a ring current of 170–200 mA. The incident flux was 10^{13} photons/s in a 0.2 mm × 1.5 mm beam footprint on the sample. Two u35 undulators were used to perform the measurements. To detect the (resonant) inelastic X-ray scattering the sample pellet was aligned to the X-ray beam at an angle of 45°. The incident X-ray energy was selected by a pair of Si crystals cut in (2 2 0) orientation. The beam was focused on a small spot (350 μm × 60 μm) on the sample. The scattered X-rays were monochromatized by the (5 3 1) Bragg planes of a spherical bent Si crystal and focused on an avalanche photodiode (APD). When scanning the energy of the scattered X-rays, the APD detector and the spherical bent Si crystal were moved concertedly in order to keep the beam spot on the sample, the bent crystal and the detector on a Rowland circle, giving an overall resolution taken from the full width at half-maximum (fwhm) of the elastic peak of 0.8 eV. A He bag was fixed between sample, analyzer crystal and detector in order to minimize

the absorption of the X-rays by air. To calibrate energy, we compared all spectra to iron foil reference, setting the first inflection of metallic iron K jump to 7111.8 eV.

In most experiments, instead of measuring the full RIXS plane, the emission energy was fixed either at the maximum of the $K\beta_{1,3}$ or the $K\beta'$ emission line and only the incident energy was scanned. The spectra are all calibrated to the incident energy scale using the elastic peak measured at the same time as the XES spectra. To determine the position of the main and satellite emission line, a Kβ emission spectrum (XES) was recorded first under non-resonant conditions, with an incident energy above the Fe K-edge at 7160 eV. Then the Fe K-edge was scanned, selecting either the $K\beta_{1,3}$ or the $K\beta'$ emission energy. Each scan had duration of 30 s–2 min, depending on the radiation damage on the samples. For the normalization purposes, EXAFS spectra were recorded on the $K\beta_{1,3}$ and the $K\beta'$ emission line and the edge jump in the XANES spectra was normalized to the edge jump in the EXAFS scans. Iron content in the samples was 0.3–0.5 wt% Fe. Comparison of transmission and fluorescence spectra of such samples showed previously that no substantial difference due to self-adsorption exists at these iron contents in the near edge region.

Radiation damage might be a serious issue, because the high incoming photon fluxes necessary to detect RIXS may induce chemical reactions in the samples. In order to minimize radiation damage, the samples were cooled to a temperature in the range 20–30 K, and the position of the beam on the sample was changed regularly between the scans. In order to be sure that the X-ray beam did not destroy the iron species under study, we checked the absence of radiation damage during the exposure time. To do it, prior to every measurement, 30 scans were performed, during 30 s each, and XANES profiles were detected. The absence of evolution within the series of the subsequent XANES spectra was applied as a criterion of stability under the beam.

3. Results and discussion

3.1. Catalytic oxidation of methane

In our previous work we have applied μ-nitrido diiron tetra(tert-butyl)phthalocyanine for the oxidation of methane [7,8]. In order to evidence that the catalytic activity is due to Fe(+3.5)NFe(+3.5) structural unit rather than due to the presence of substituents and the μ-nitrido diiron complexes on the unsubstituted phthalocyanine platform can be used as model complexes we have checked the catalytic properties of **1**. Heterogeneous oxidation of methane by H_2O_2 was performed in the presence of supported catalyst **1**-SiO_2 in aqueous solution containing 0.075 M sulphuric acid at 60 °C. These conditions were found to be optimal for the high catalytic activity [8]. The reaction was performed in autoclave at 32 bar CH_4 using 1:685 catalyst to oxidant ratio during 20 h. The aqueous solution recovered after reaction contained 5.8 mM and 40.5 mM concentrations of formaldehyde and formic acid, respectively. The total turnover number was determined to be 102.9 ($TON_{CH_2O} = 12.9$, $TON_{HCOOH} = 90$) compared with TON = 209 in the case of supported μ-nitrido diiron tetra(tert-butyl)phthalocyanine [8]. Taking into account the stoichiometry of methane oxidation to formaldehyde and formic acid, 43% yield on H_2O_2 was achieved. Thus, μ-nitrido diiron phthalocyanine efficiently catalyzes methane oxidation although its catalytic activity is somewhat lower than that of tert-butyl substituted counterpart. We have therefore demonstrated that unusually high oxidative power is not a unique property of the tert-butyl substituted compound reported earlier, but seems to be a general property of diiron phthalocyanine nitrido dimers.

3.2. EPR study

Prior to the X-ray spectroscopy study, all the synthesized complexes were characterized by the X-band EPR spectroscopy. Monomeric 6-coordinated iron phthalocyanines are usually low spin species while 5-coordinated complexes are either high spin ($S = 5/2$) or intermediate or spin-admixed species ($S = 5/2/S = 3/2$) [31]. FePcCl showing $g = 4.67$ and $g = 2.0$ signals has low-lying high-spin state admixed to ground state [32]. Both unsubstituted and tert-butyl substituted diiron compounds containing the $Fe^{+3.5}$(μ-N)$Fe^{+3.5}$ core showed intense axial signals of low-spin ($S = 1/2$) $3d^5$ Fe(III) with *g*-factors near 2. These signals are described in detail in the earlier literature and in our recent study [14]. The two-electron oxidized compound **3** demonstrated a very intense signal of cation radical species, in which the unpaired electron is localized at the phthalocyanine ring [14]. The one-electron oxidized compound **2**, presumably containing the Fe^{IV}(μ-N)Fe^{IV} core was EPR-silent. This might be explained in different ways: either the Fe^{IV} species have zero field splitting not compatible with observation of EPR spectra, or two iron centers ($S = 1$ or $S = 2$) are antiferromagnetically coupled making the whole molecule EPR-silent. This dilemma cannot be resolved on the basis of sole EPR spectroscopy; in any case the EPR observations of d^4 configuration are quite rare.

3.3. X-ray scattering and emission spectroscopy

3.3.1. XES main Kβ lines

In the high resolution K fluorescence emission spectra a hole in the 1s shell is first created and the photons are emitted due to decay of hole by dipole-allowed relaxation from the *n*p ($n = 2, 3$) levels (Scheme 1). The 3p–1s transitions denoted as Kβ lines are considered in this work. The electronic state with a 1s core hole is called the intermediate state. The final state reached when the 1s vacancy is filled, contains a 3p hole. The interaction of 3p hole with partially filled levels of central atom explains chemical sensitivity of high resolution XES spectroscopy [29,30]. The chemical sensitivity is enhanced due to the spin sensitivity of the main Kβ lines and sensitivity of satellites lines to the nature of ligands.

Nonresonant X-ray emission spectra were recorded by setting the incident energy above the K absorption edge. In the case of non-resonant XES both $K\beta_{1,3}$ and $K\beta'$ features are spin-allowed whatever the spin state of Fe atom. The final state $3p^5$ is split by the exchange interaction between the 3p hole and the spin-unpaired 3d electrons of iron (as depicted for resonant emission in Scheme 1, at the left). The Kβ fluorescence spectrum contains an intense line ($K\beta_{1,3}$) at 7059 eV (broadened at the low energy side owing to multi-electron shake-up effects) and a weaker line $K\beta'$ at 7045 eV. The $K\beta'$ line appears due to antiparallel orientation between the spins of the 3p hole and the 3d electrons [33]. In the non-resonant XES any spin orientation of excited electron is possible, whereas for the resonant case spin orientation of excited electron might be constrained or even fixed due to the electrons present on partially occupied 3d orbitals (compare different number of spin-up and spin down excitation-decay RIXS events depicted respectively with red and blue in Scheme 1).

It was observed that the position of main XES lines is determined mostly by the number of unpaired electrons on the d-levels [30]. Due to the short range of 3p–3d exchange interactions, this line position depends on the local effective 3d spin density on the central atom and is not affected by the interactions with other spins in the molecule (or solid). The local 3d spin density depends obviously on the Fe oxidation state, but might be affected by ligand environment, causing LS–HS transitions. Otherwise it depends on the mixing with the ligands orbitals via charge transfer from the filled orbitals of ligand to the empty 3d iron orbitals, or vice versa.

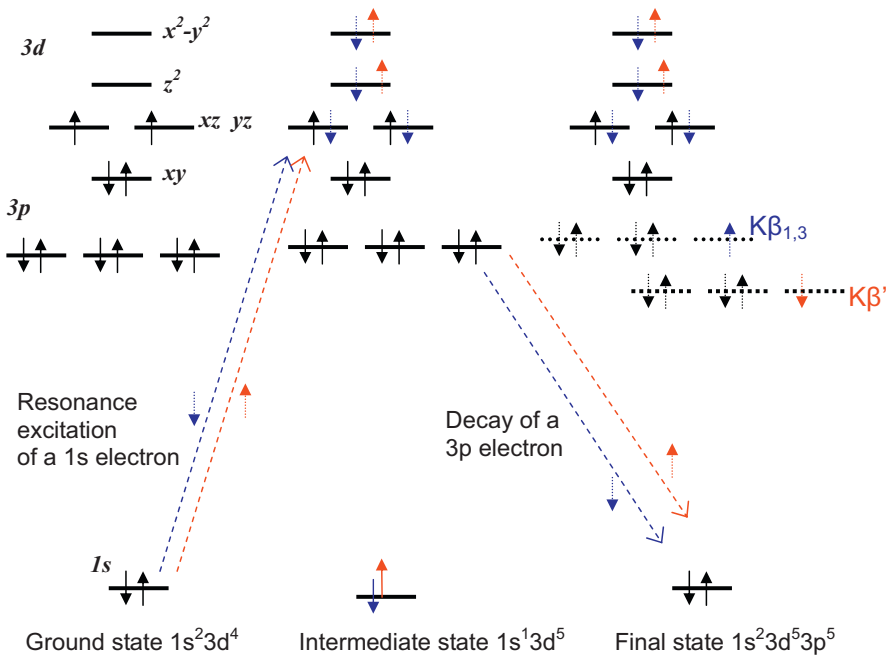

Scheme 1. RIXS processes for a d^4 C_{4v} configuration. Red and blue arrows represent alternative one-electron events for the Kβ′ and $Kβ_{1,3}$ processes, respectively. The intensity of resonant events depends on the number of intermediate states available for each process. (For interpretation of the references to color in this scheme legend, the reader is referred to the web version of the article.)

The nonresonant XES spectra of the compounds under study are represented in Fig. 2. The complexes **1** and **3** demonstrate similar spectra typical for the low-spin Fe species having low intensity of the Kβ′ line which is merged with the shoulder of the main line. Note that both compounds **1** and **3** have one unpaired EPR-active electron, but its localization should be supposed to be quite different: on $Fe^{+3.5}$(μ-N)$Fe^{+3.5}$ core in **1** and on phthalocyanine ligand in **3**. However, this does not affect the observed XES spectra. Moreover, the difference of formal oxidation state of iron in these compounds does not appreciably affect the shape of XES lines. Monomeric iron phthalocyanine taken as reference, shows a well-separated Kβ′ and $Kβ_{1,3}$ lines, typical for the $S = 5/2$ configuration [30]. Comparison of FePcCl spectrum to that of one-electron oxidized dimer **2**, shows a 1.0 eV decrease in energy upon which may be attributed to the decrease in spin state from $S = 5/2$ to $S = 2$.

When passing from **1** to one-electron oxidized **2** and then to two-electron oxidized **3**, the XES spectra change in an irregular manner. For neutral **1** and doubly charged **3** similar spectra typical for LS iron were observed whereas the intermediate between them species **2** showed a HS-type spectrum, similar but not identical to the spectrum of Fe $3d^5$, presumably because of $S = 2$ state.

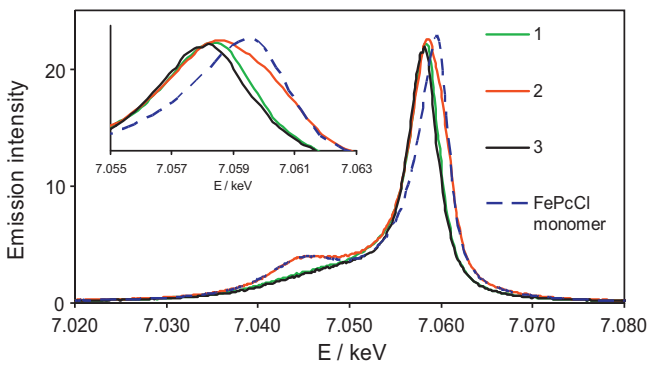

Fig. 2. Main Kβ XES lines of the μ-nitrido dimer **1**, one-electron **2** and two-electron **3** oxidized compounds, and reference monomer FePcCl.

Hypothetically this counter-intuitive behaviour might be explained by weakening of covalent interaction in the Fe(μ-N)Fe core, which might occur if the bridging nitrogen bears a significant positive charge changing its hybridization.

Noteworthily, the center of gravity of the XES spectra, was not significantly different in the studied samples. This corroborates the conclusion that the shifts in the positions of the Kβ lines are mostly caused by variations in the exchange splitting [29]. Supposing the freezing of the valence shell orbital angular momentum and neglecting spin–orbit interactions, a linear relation between the exchange splitting and the spin in the metal 3d shell was suggested [34]. Overall, our XES results suggest an unexpected LS–HS–LS transition in the sequence initial dimer **1** – one-electron oxidized **2** – two-electron oxidized **3**.

3.3.2. *Kβ satellite lines*

Kβ satellite lines appear due to the valence-to-core transitions, mostly due to relaxation of an electron to the 1s hole from the ligand ns (Kβ″ or 'cross-over' peak) and 4p orbitals ($Kβ_{2,5}$ peak), as well as possibly due to the 3d–1s transitions. Therefore these features are the most chemically sensitive fluorescence lines. However the complexity of many-electron effects responsible for the shape of $Kβ_{2,5}$ features makes their straightforward comparison difficult. Recently TDFT calculations were successfully applied to predict the shape of satellite lines of a sequence of model iron compounds and therefore to probe the valent atomic orbitals [28]. Such calculations are in progress for our systems, but in this work we provide only a qualitative discussion, which resumes to a simple conclusion as follows.

The Kβ″ peak can be assigned to ligand 2s to iron 1s cross-over transitions, its position depending on the 2s binging energy of the ligand and its intensity decreasing exponentially with the iron–ligand distance [35]. The relative shifts between the cross-over fluorescence energies for different ligands correspond mainly to the shifts in 2s binding energies of the atomic species.

All the dimeric species show a cross over line at 7097 eV, unlike monomeric complex, in agreement with their molecular structure

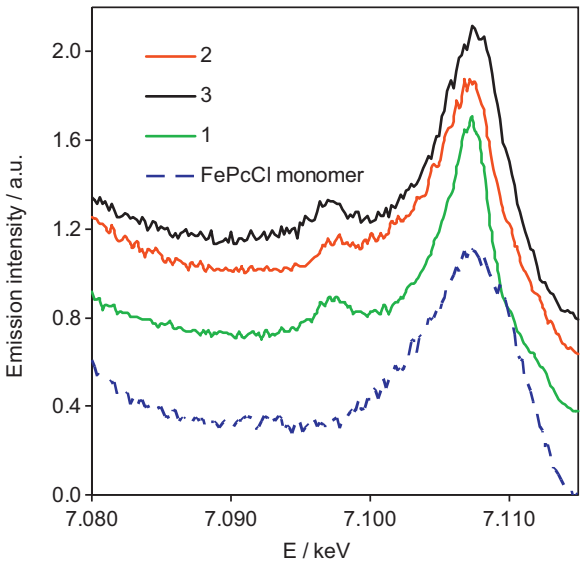

Fig. 3. Kβ satellite spectra for samples **1**–**3**, and reference FePcCl.

(Fig. 3). Indeed, a short axial Fe–N bond exists in the dimer which introduces Kβ″ peak due to a stronger overlap between Fe 3d and N 2s orbitals. Dimeric structure is therefore preserved after oxidation in all the complexes studied. The intensity varies slightly and seems to be lower in one-electron oxidized complex **2**. That might be due to a positive charge partially localized on nitrogen and thus decreasing the Fe 3d to N 2s overlap. However this statement remains a hypothesis, because at the background level present in our experimental curves the uncertainty is too high to state it definitely.

3.3.3. *Conventional XANES*

Local electronic structure of iron can be addressed by inspection of the pre-edge region which arises from the excitations of 1s electrons into the lowest unoccupied 3d electronic states. The K pre-edge of iron is sensitive to the oxidation state, the site symmetry and the crystal field splittings [36]. The most useful characteristics of the Fe–K pre-edge for determining Fe oxidation state and coordination number are the position of its centroid and its integrated intensity. Generally, the pre-edge intensity increases with lowering the coordination shell symmetry and with the introduction of close-standing ligands. The increase of pre-edge intensity is particularly strong when passing from octahedral to tetrahedral iron coordination, as the greater the deviation of the site from centrosymmetry, the greater the intensity of the ls–3d transition feature [37]. The pre-edge arises from 1s–3d quadrupolar transitions only in systems with strict inversion symmetry. If this symmetry is not present, as for the molecules studied here, then p–d orbital mixing can occur, and the pre-edge features can become dominated by 1s–4p dipolar transitions. XANES spectra of compounds **1**–**3** and relevant FePc monomer are presented in Fig. 4.

The centroid position (first moment of the pre-edge curve) is around 7113.7 eV for Fe(III) (FePcCl), 7113.8 for Fe(3.5+) (compound **1**) and Fe(IV) (compound **2**), whereas it raised to 7114.7 eV for the Fe(IV) compound **3**. The values of the pre-edge centroid for the products containing Fe(III) are in satisfactory agreement with those of Fe(III) reference oxide compounds (~7113.5 eV, [38]). Note however that care must be taken in the interpretation of the pre-edges of different classes of compounds, since the pre-edge position does not depend straightforwardly on the oxidation degree, but rather on the splitting and occupation of the 3d levels as well as on the real electron density on the Fe site which is only loosely

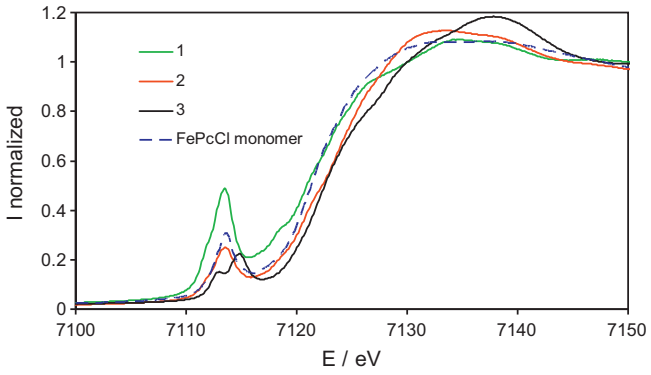

Fig. 4. Conventional XANES spectra of the compounds **1**–**3** and of the monomer FePcCl.

correlated to the formal oxidation state. No clear evolution of pre-edge position is found in the sequence of three spectra of FePcCl, **1** and **2**. Only in the compound **3** the pre-edge shifts significantly towards higher energy.

Earlier, for Fe(II) and Fe(III) phthalocyanines, an expected shift of the main jump and the pre-edge with the increase of oxidation degree was noted [39], however XAS spectra of higher oxidation degrees iron phthalocyanines were not studied systematically. The data presented here are in good agreement with our previous work on similar compounds [10,11], beside one-electron oxidized compound **2** which was never studied by XAS and appears to have pre-edge position similar to those of Fe(III) monomer and intermediate valence dimer **1**. The intensity of the pre-edge strongly decreases from FePcCl to **1** due to the introduction of a short Fe–N bond in the axial position, then again it decreases in **2** and **3**, probably due to partial symmetrization of iron environment by coordinating counteranions (indeed, the compound **1** is neutral and Fe can have square pyramidal coordination in it, whereas **2** and **3** are ionic and therefore counteranions should be present, changing iron coordination to distorted octahedral).

As with main jump position it changes somewhat differently than the position of pre-edge. The main jump energy expectedly increases from lower to higher oxidation states. For FePCl and **1** it corresponds to ca 7122.1 eV at the point of maximal derivative. As far as Fe(IV) become main species (compounds **2** and **3**), the main jump position becomes 7123.5 eV. Again, the main jump represents by no means a straightforwardly quantifiable single one-electron event, but a lump of complex events, and therefore its position might be used only as a general guideline. As a conclusion it can be stated that while conventional XANES provides valuable information on the general trends in the evolution of iron species, but it might become misleading in cases when several parameters change at once, such as geometry and oxidation state, as it probably happens in the sequence of compounds under study.

3.3.4. *Spin-selective XANES spectra*

The K pre-edge in the conventional absorption spectroscopy, though useful, is sometimes difficult to interpret since the pre-edge often is strongly overlapped with the main edge and not resolved sufficiently. Compared to the conventional XANES spectra, the Kβ-detected spectra are better resolved due to the line-sharpening effect [40]. Moreover, comparison of $K\beta_{1,3}$-detected vs. Kβ′-detected spectra can allow unravelling the issues of occupancy of the electronic orbital manifold, not accessible by conventional XANES. Spin-selective XANES spectra at the Fe K edge were recorded by fixing the recorded emission energy respectively at the maximum of the $K\beta_{1,3}$ emission line (7059 eV) and at the Kβ′ line (7045 eV), and then by scanning the incident energy within the usual ranges of XANES observation. The XANES spectra of the

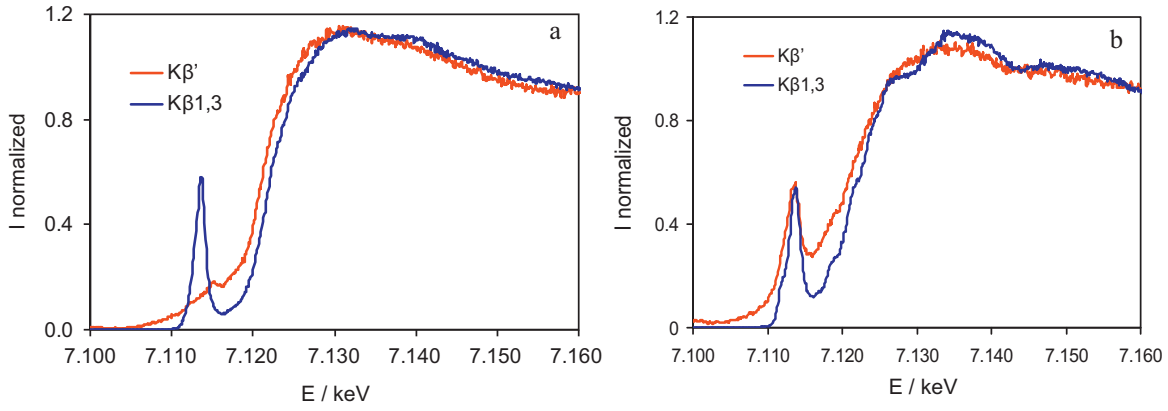

Fig. 5. Spin selective XANES spectra of the monomer FePcCl (a) and μ-nitrido dimer **1** (b). All intensities are normalized to unit main jump.

compounds under study recorded at the maximum of $K\beta_{1,3}$ emission line and at the Kβ′ line are shown in Figs. 5–7.

For high spin Fe(III) configuration $3d^5$, all the 3d orbitals are partially occupied with spin up electrons. Therefore only spin-down 1s electron can jump to the 3d state in the pre-edge region. As a consequence only a down-spin 1s hole is created and a spin-down 3p electron can fill this vacancy. $K\beta_{1,3}$ emission is the only possibility in the pre-edge region for this electronic configuration (cf. Scheme 1). Therefore no pre-edge is observed in the XANES spectrum recorded at the Kβ′ emission energy (Fig. 5a). By contrast, at the $K\beta_{1,3}$ emission incident energy, an intense pre-edge feature can be observed and it is usually better resolved in the resonant spectra than in the conventional XANES.

Already a qualitative visual analysis of the spectra is sufficient to make general conclusions. Thus, a striking difference is revealed by spin-selective XANES between the compounds **1** and **2** and FePcCl monomer, having otherwise similar pre-edge features conventional XANES (cf. Figs. 4 and 5). Somewhat more rigorous treatment includes subtraction of polynomial background (Fig. 6a) and decomposition of the spectra to superposition of Voigt amplitude components (Fig. 6b). The following discussion is based on such analysis and the data of pre-edge representation as a superposition of symmetric Voigt profiles are summarized in Table 1. Note that in the case of Kβ′-detection the background might contain electronic contributions [41]. However, quantum mechanical simulation of the pre-edges is beyond the scope of this work and will be published elsewhere.

For the monomer FePcCl a seemingly single strong pre-edge peak was observed at $K\beta_{1,3}$ energy, at 7113.8 eV. However this peak is asymmetric and should be represented as a superposition of two components respectively at 7112.6 and 7113.8 eV with an area ratio 1:5. By contrast in the Kβ′ detected spectrum the pre-edge region shows almost negligible intensity and originated rather from limited detection accuracy than from real Kβ′ event. This is naturally explained by supposing $S = 5/2$ spin state of iron, in which case all the orbitals are partially occupied and resonant Kβ′ process is spin-forbidden. Therefore, spin selective spectra give a straightforward evidence of the high spin configuration d^5 in the monomer FePcCl.

The situation drastically changes when passing from the monomer to dimer compound **1**. In this case XANES profiles detected at two emission energies, differ only slightly (Fig. 5b) indicating low 3d spin density on the Fe atoms (probably $S = 1$) implying sufficient number of empty 3d levels to provide a high

Table 1
Analysis of the pre-edge feature in the dimeric μ-nitrido complexes and reference FePcCl.

Sample	Type of detection	Components energy, eV (area, for the spectra normalized to unit main jump)
FePcCl	$K\beta_{1,3}$	7112.6 (0.061); 7113.8 (0.21)
	Kβ′	7115.0 (0.019)
1	$K\beta_{1,3}$	7112.3 (0.066); 7113.9 (0.24)
	Kβ′	7112.3 (0.061); 7113.8 (0.22)
2	$K\beta_{1,3}$	7112.1 (0.031); 7113.9 (0.13)
	Kβ′	7112.1 (0.022); 7113.8 (0.051)
3	$K\beta_{1,3}$	7113.0 (0.050); 7115.1 (0.11)
	Kβ′	7112.9 (0.062); 7115.0 (0.090)

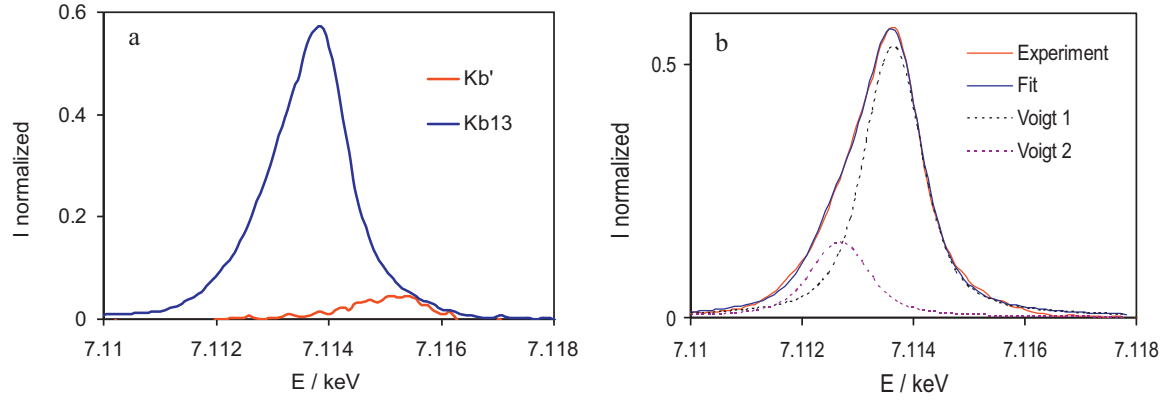

Fig. 6. Pre-edge feature for the monomeric FePcCl measured at different emission lines after background subtraction (a) and decomposition of $K\beta_{1,3}$ pre-edge peak to Voigt profiles for the FePcCl (b).

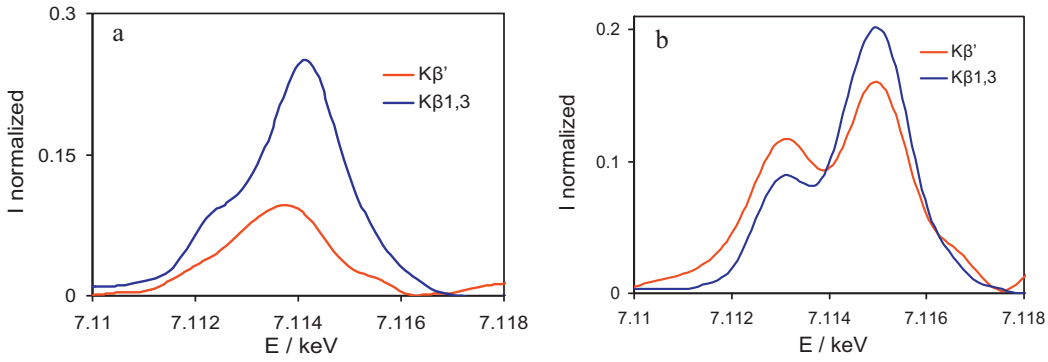

Fig. 7. Pre-edge peaks of the complexes **2** (a) and **3** (b), measured at different emission energies.

intensity resonant pre-peak (Scheme 1). Two components are necessary to describe the spectra in both cases, and their positions are close for two modes of detection.

In the oxidized complexes **2** and **3** the normalized intensity of pre-edge feature was strongly decreased as compared to the dimer **1** and monomer FPcCl (Table 1). This might be due to a relative symmetrization of iron environment, changing from tetragonal pyramidal (C_{4v}) in **1** and FePcCl to distorted octahedral one in **2** and **3**. Due to such a symmetrization the matrix elements of dipole allowed transitions with the participation of 4p-ligand orbitals should be decreased.

The spectra of oxidized complexes **2** and **3** are significantly different. Most importantly, for the complex **2** a strong decrease of Kβ′-detected pre-edge intensity was observed, consistently with its supposed highest spin $S=2$, suggested from the XES spectra (Fig. 7a). Similarly to the monomer FePcCl the components are not resolved, probably due to the abundance of multiple configurations. By contrast, the spectra of two-electron oxidized **3** correspond clearly to the low-spin $S=1$ configuration, because of small difference between the XANES pre-edges detected on two XES lines, consisting merely in some redistribution between the high-and low-energy components, without change of integral intensity (cf. Table 1 and Fig. 7b).

It has been shown earlier for Fe(II) complexes that the splitting of pre-edge components increases when the local geometry changes from tetrahedral to octahedral [37]. At the same time the intensity of pre-edge feature is decreased. In our case, the mean splitting is 1.55 eV, 1.75 eV and 2.1 eV for compounds **1**, **2** and **3** respectively. The intensity of the pre-edge feature decreases in the same sequence. This observation corroborates general rule that symmetrization of environment and concomitant increase of orbitals splitting occurs in the series **1**–**3**. Further analysis shows that the relative intensity of high-energy component for **2** and **3** is systematically decreased in the Kβ′-detected spectrum. This result is somewhat counter-intuitive. Indeed, whatever the exact topology and filling of the electronic orbitals, those orbital levels which are empty are obviously higher lying than those which are partially filled. At the same time only the empty 3d orbitals can be involved

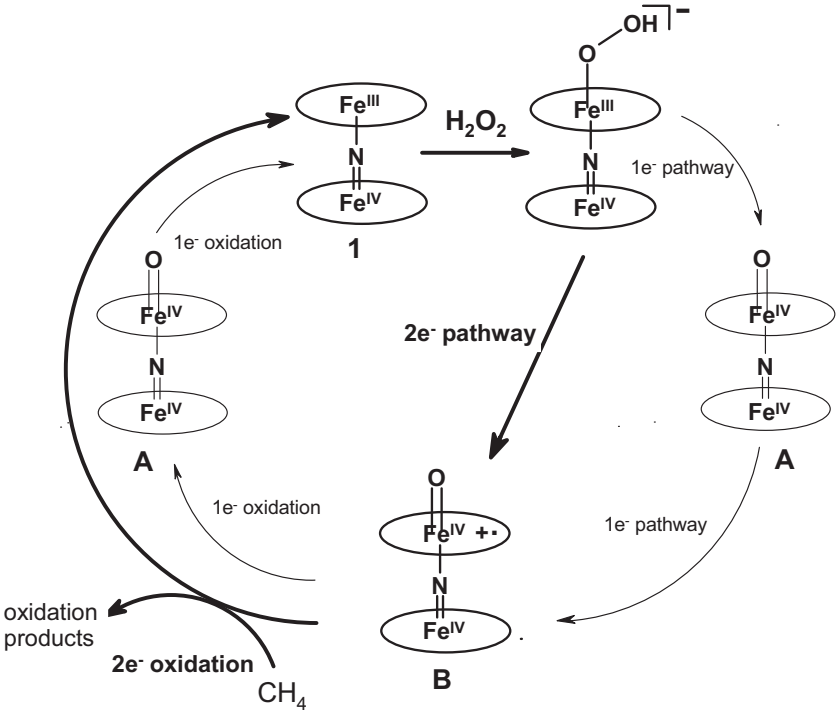

Fig. 8. Proposed mechanism of the formation of active species in the PcFe(μ-N)FePc–H_2O_2 system involving the initial complex **1**, the oxo complexes **A** and **B**, modelled in this study by complexes **2** and **3**, respectively. Principal pathways are indicated in bold style.

in the Kβ′-detected pre-edge, whereas both empty and partially filled orbitals may participate in the $K\beta_{1,3}$-detected one. From this qualitative consideration, Kβ′-detected pre-edge should have higher (or equal) intensity as compared to the $K\beta_{1,3}$-detected one. To resolve this contradiction simulations using (time-dependent) DFT approach is underway, and it will be published as a separate dedicated work.

In summary, spin states and oxidation states of iron in the Fe(μ-N)Fe series were probed by XES/spin selective XAS. $Fe^{+3.5}$(μ-N)$Fe^{+3.5}$ and Fe^{IV}(μ-N)Fe^{IV} configurations have been evidenced and local spin density on iron was addressed in this study.

A tentative explanation of the HS configuration for one-electron oxidized complex **2** can be given. Probably due to particular stability of $3d^5$ manifold, the $3d^4$ configuration tends to have an admixture of $3d^5L^+$ (where L^+ represents a hole on the ligand). This configuration is less favorable for two-electron oxidized complex **3** where ligand already bears a significant positive charge and is reluctant to donate additional (second) electron to iron. This might be the key to high oxidizing activity of the Fe(IV) complexes in general. Indeed, monomeric iron(IV)–oxo sites may exist in triplet or quintet ground states. The model Fe(IV) complexes often have lower spin [42] though some quintet state complexes were also reported [43]. In the nonheme enzymes iron active sites usually demonstrate quintet spin configuration [44]. DFT calculations predict higher reactivity of $S = 2$ iron (IV)–oxo intermediates towards C–H bond activation as compared to the corresponding $S = 1$ species [45,46]. The dimeric structure probably brings out resonance stabilization of high-valent species.

Possible pathways of the formation of active species in the PcFe(μ-N)FePc–H_2O_2 system are indicated in Fig. 8.

Supposing that one-electron and two-electron oxidized species in this system follow the same trends as observed in this study model compounds **1**–**3** one can suggest that the two-electron oxidation should be the main pathway for the formation of the active species via heterolytic cleavage of O–O bond. The direct formation of low spin $[PcFe^{IV}(\mu\text{-}N)Fe^{IV}(O)(Pc^{\bullet+})]^0$ from low spin $[PcFe^{+3.5}(\mu\text{-}N)Fe^{+3.5}(Pc)]^0$ in two-electron process is more favorable than its formation via two successive one-electron oxidations to avoid LS–HS–LS transformations. For the same reason the formation of high spin $[PcFe^{IV}(\mu\text{-}N)Fe^{IV}(O)Pc]^-$ from low spin $[PcFe^{+3.5}(\mu\text{-}N)Fe^{+3.5}(Pc)]^0$ is less favorable. Thus, due to the favorable electronic structure a powerful oxidizing species $[PcFe^{IV}(\mu\text{-}N)Fe^{IV}(O)(Pc^{\bullet+})]^0$ can be formed. The electronic structures of the resting complex $[PcFe^{+3.5}(\mu\text{-}N)Fe^{+3.5}(Pc)]^0$, one-electron oxidized $[PcFe^{IV}(\mu\text{-}N)Fe^{IV}(O)Pc]^-$ and two-electron oxidized $[PcFe^{IV}(\mu\text{-}N)Fe^{IV}(O)(Pc^{\bullet+})]^0$ species could also influence the oxidation pathways in the system. In principal, $[PcFe^{IV}(\mu\text{-}N)Fe^{IV}(O)(Pc^{\bullet+})]^0$ can oxidize substrates via one-electron or two-electron reactions. The latter pathway from LS to LS states should be favored with respect to LS–HS–LS transformation. In this way, methane is oxidized to methanol which being much more reactive than methane further undergoes oxidation to formaldehyde and finally to formic acid.

4. Conclusion

The origin of powerful oxidizing properties of N-bridged diiron phthalocyanines capable of oxidizing methane under very mild near ambient conditions is of great interest. To get an insight in the properties of these emerging oxidation catalysts we have studied a row of three model complexes in three oxidation states related to different species in the catalytic cycle. The main novel result is that in the series of model compounds unexpected LS–HS–LS transition was detected when changing oxidation state in the row from the initial $[PcFe^{+3.5}NFe^{+3.5}Pc]^0$ complex to $[PcFe^{IV}NFe^{IV}Pc]^+PF_6$ and then to $[PcFe^{IV}NFe^{IV}(Pc^{\bullet+})]^{2+}Br_2$. This finding can explain preferential two-electron pathway for the formation of the strong species oxidizing methane via two-electron oxidation. In addition, we have demonstrated the potential of 1s3p RIXS spectroscopy for characterization of Fe phthalocyanine complexes. The 1s3p RIXS enables to separate out the lowest K-edge resonances of preedge features. This work provides rare XES and RIXS data for Fe(IV) complexes which can be used as a benchmark for usually unstable Fe(IV) species related to biochemical and biomimetic oxidations. The sensitivity of RIXS is high enough to examine the state of iron in the diluted reaction mixtures. Since RIXS is carried out using hard X-rays, it is highly appropriate for operando measurements. Therefore our further effort will be directed on the in situ studies of homogeneous reaction mixtures and supported complexes.

Acknowledgements

We are grateful to Agence National de Recherche (ANR, France, grant ANR-08-BLANC-0183-01) for financial support of this research. We acknowledge the European Synchrotron Radiation Facility (Grenoble, France) for provision of ID26 beam line.

References

[1] A. Holmen, Catal. Today 142 (2009) 2–8.
[2] L. Olivier, S. Haag, C. Mirodatos, A.C. van Veen, Catal. Today 142 (2009) 34–41.
[3] B. Vora, J.Q. Chen, A. Bozzano, B. Glover, P. Barger, Catal. Today 141 (2009) 77–83.
[4] A.E. Shilov, G.B. Shul'pin, Chem. Rev. 97 (1997) 2879–2932.
[5] R.A. Periana, D.J. Taube, S. Gamble, H. Taube, T. Satoh, H. Fujii, Science 280 (1998) 560–564.
[6] R. Palkovits, C. von Malotki, M. Baumgarten, K. Müllen, C. Baltes, M. Antonietti, P. Kuhn, J. Weber, A. Thomas, F. Schüth, ChemSusChem 3 (2010) 277–282.
[7] A.B. Sorokin, E.V. Kudrik, D. Bouchu, Chem. Commun. (2008) 2562–2564.
[8] A.B. Sorokin, E.V. Kudrik, L.X. Alvarez, P. Afanasiev, J.M.M. Millet, D. Bouchu, Catal Today 157 (2010) 149–154.
[9] E.V. Kudrik, A.B. Sorokin, Chem. Eur. J. 14 (2008) 7123–7126.
[10] P. Afanasiev, D. Bouchu, E.V. Kudrik, J.M.M. Millet, A.B. Sorokin, Dalton Trans. (2009) 9828–9836.
[11] Ü. İşci, P. Afanasiev, J.M.M. Millet, E.K. Kudrik, V. Ahsen, A.B. Sorokin, Dalton Trans. (2009) 7410–7420.
[12] E.V. Kudrik, P. Afanasiev, D. Bouchu, J.M.M. Millet, A.B. Sorokin, J. Porphyrins Phthalocyanines 12 (2008) 1078–1089.
[13] Ü. İşci, F. Dumoulin, V. Ahsen, A.B. Sorokin, J. Porphyrins Phthalocyanines 14 (2010) 324–334.
[14] P. Afanasiev, E.V. Kudrik, J.M.M. Millet, D. Bouchu, A.B. Sorokin, Dalton Trans. 40 (2011) 701–710.
[15] M.-H. Baik, M. Newcomb, R.A. Friesner, S.J. Lippard, Chem. Rev. 103 (2003) 2385–2419.
[16] B. Meunier, S.P. de Visser, S. Shaik, Chem. Rev. 104 (2004) 3947–3980.
[17] L.A. Bottomley, J.-N. Gorce, V.L. Goedken, C. Ercolani, Inorg. Chem. 24 (1985) 3733–3737.
[18] B. Floris, M.P. Donzello, C. Ercolani, Single-atom bridged dinuclear metal complexes with emphasis on phthalocyanine systems, in: K.M. Kadish, K.M. Smith, R. Guilard (Eds.), Porphyrin Handbook, vol. 18, Elsevier Science, San Diego, 2003, pp. 1–62.
[19] C. Ercolani, M. Gardini, G. Pennesi, G. Rossi, U. Russo, Inorg. Chem. 27 (1988) 422–424.
[20] R. Sarangi, R.K. Hocking, M.L. Neidig, M. Benfatto, T.R. Holman, E.I. Solomon, K.O. Hodgson, B. Hedman, Inorg. Chem. 47 (2008) 11543–11550.
[21] J.F. Lin, V.V. Struzhkin, S.D. Jacobsen, M.Y. Hu, P. Chow, J. Kung, H. Liu, H.-K. Mao, R.J. Hemley, Nature 436 (2005) 377–380.
[22] G.D. Pirngruber, J.-D. Grunwaldt, P.K. Roy, J.A. van Bokhoven, O. Safonova, P. Glatzel, Catal. Today 126 (2007) 127–134.
[23] D.C. Radu, P. Glatzel, W.M. Heijboer, J.H. Bitter, B.M. Weckhuysen, F.M.F. de Groot, Stud. Surf. Sci. Catal. 170 (2007) 796–799.
[24] S.A. Suchkova, A. Soldatov, K. Dziedzik-Kocurek, M.J. Stillman, J. Phys.: Conf. Ser. 109 (2009) 012211.
[25] X. Sheng, J.H. Horner, M. Newcomb, J. Am. Chem. Soc. 130 (2008) 13310–13320.
[26] T.A. Jackson, J.U. Rohde, M.S. Seo, C.V. Sastri, R. DeHont, A. Stubna, T. Ohta, T. Kitagawa, E. Münck, W. Nam, L. Que Jr., J. Am. Chem. Soc. 130 (2008) 12394–12407.
[27] A. Mijovilovich, W. Meyer-Klaucke, J. Synchr. Rad. 10 (2003) 64–68.
[28] N. Lee, T. Petrenko, U. Bergmann, F. Neese, S. DeBeer, J. Am. Chem. Soc. 132 (2010) 9715–9727.
[29] F. De Groot, Chem. Rev. 101 (2001) 1779–1808.
[30] P. Glatzel, U. Bergmann, Coord. Chem. Rev. 249 (2005) 65–95.
[31] B.J. Kennedy, K.S. Murray, H. Homborg, W. Kalz, Inorg. Chim. Acta 134 (1987) 19–21.

[32] B.J. Kennedy, K.S. Murray, P.R. Zwack, H. Homborg, W. Kalz, Inorg. Chem. 25 (1986) 2539–2545.
[33] X. Wang, C.R. Randall, G. Peng, S.P. Cramer, Chem. Phys. Lett. 243 (1995) 469–473.
[34] P. Glatzel, Ph.D. Thesis, Hamburg University, Hamburg, 2001.
[35] U. Bergmann, C.R. Horne, T.J. Collins, J.M. Workman, S.P. Cramer, Chem. Phys. Lett. 302 (1999) 119–124.
[36] T.E. Westre, P. Kennepohl, J.G. DeWitt, B. Hedman, K.O. Hodgson, E.I. Solomon, J. Am. Chem. Soc. 119 (1997) 6297–6314.
[37] W.E. Jackson, F. Farges, M. Yeager, P.A. Mabrouk, S. Rossano, G.A. Waychunas, E.I. Solomon, G.E. Brown, Geochim. Cosmochim. Acta 69 (2005) 4315–4332.
[38] M. Wilke, F. Farges, P.-E. Petit, G.E. Brown, F. Martin, Am. Mineral. 86 (2001) 714–730.
[39] S.Y. Ha, J. Park, T. Ohta, G. Kwag, S. Kim, Electrochem. Solid State Lett. 2 (1999) 461–464.
[40] H. Hayashi, T. Azumi, A. Sato, Y. Udagawa, J. Electron. Spectrosc. Relat. Phenom. 168 (2008) 34–39.
[41] H. Yamaoka, M. Oura, M. Taguchi, T. Morikawa, K. Takahiro, A. Terai, K. Kawatsura, A.M. Vlaicu, Y. Ito, T. Mukoyama, J. Phys. Soc. Jpn. 73 (2004) 3182–3191.
[42] W. Nam, Acc. Chem. Res. 40 (2007) 522–531.
[43] J. England, M. Martinho, E.R. Farquhar, J.R. Frisch, E.L. Bominaar, E. Münck, L. Que Jr., Angew. Chem. Int. Ed. 48 (2009) 3622–3626.
[44] C. Krebs, D.G. Fujimori, C.T. Walsh, J.M Bollinger Jr., Acc. Chem. Res. 40 (2007) 484–492.
[45] S. Shaik, H. Hirao, D. Kumar, Acc. Chem. Res. 40 (2007) 532–542.
[46] C. Geng, S. Ye, F. Neese, Angew. Chem. Int. Ed. 49 (2010) 5717–5720.